Alterations of cellular bioenergetics in pulmonary artery endothelial cells

Weiling Xu*, Thomas Koeck*, Abigail R. Lara†, Donald Neumann‡, Frank P. DiFilippo‡, Michelle Koo*, Allison J. Janocha*, Fares A. Masri*, Alejandro C. Arroliga†, Constance Jennings†, Raed A. Dweik*†, Rubin M. Tuder§, Dennis J. Stuehr*, and Serpil C. Erzurum*†¶

Departments of *Pathobiology, †Pulmonary and Critical Care Medicine, and ‡Nuclear Medicine, Cleveland Clinic, Cleveland, OH 44195; and §Division of Cardiopulmonary Pathology, The Johns Hopkins University School of Medicine, Baltimore, MD 21205

Edited by Salvador Moncada, University of London, London, United Kingdom, and approved December 1, 2006 (received for review June 17, 2006)

Idiopathic pulmonary arterial hypertension (IPAH) is pathogenetically related to low levels of the vasodilator nitric oxide (NO). Because NO regulates cellular respiration and mitochondrial biogenesis, we hypothesized that abnormalities of bioenergetics may be present in IPAH. Evaluation of pulmonary artery endothelial cells from IPAH and control lungs *in vitro* revealed that oxygen consumption of IPAH cells was decreased, especially in state 3 respiration with substrates glutamate-malate or succinate, and this decrease paralleled reduction in Complex IV activity and IPAH cellular NO synthesis. IPAH pulmonary artery endothelial cells had decreased mitochondrial dehydrogenase activity and lowered mitochondrial numbers per cell and mitochondrial DNA content, all of which increased after exposure to NO donors. Although IPAH/pulmonary artery endothelial cells' ATP content was similar to control under normoxia, cellular ATP did not change significantly in IPAH cells under hypoxia, whereas ATP decreased 35% in control cells, identifying a greater dependence on cellular respiration for energy in control cells. Evidence that glucose metabolism was subserving the primary role for energy requirements of IPAH cells was provided by the ≈3-fold greater glycolytic rate of IPAH cells. Positron emission tomography scan with [^{18}F]fluoro-deoxy-D-glucose performed on IPAH patients and healthy controls revealed significantly higher uptake in IPAH lungs as compared with controls, confirming that the glycolytic rate was increased *in vivo*. Thus, there are substantial changes in bioenergetics of IPAH endothelial cells, which may have consequences for pulmonary hypertensive responses and potentially in development of novel imaging modalities for diagnosis and evaluation of treatment.

cellular respiration | nitric oxide | oxygen consumption | pulmonary hypertension | mitochondrion

Idiopathic pulmonary arterial hypertension (IPAH) is a fatal disease of unknown etiology characterized by a progressive increase in pulmonary artery pressure and vascular growth (1, 2). Secondary forms of pulmonary arterial hypertension (PAH) are associated with known diseases, such as collagen vascular diseases or portal hypertension but in the absence of an identifiable etiology are classified as IPAH. Abnormalities in vasodilators, specifically nitric oxide (NO), have been implicated in the pathogenesis of pulmonary hypertension (1–5). NO is produced in the lung by NO synthases (NOS; EC 1.14.13.39) (6–8). There is conclusive evidence from animal models of pulmonary hypertension, mice genetically deficient in endothelial NOS (eNOS), and complementation studies with gene transfer of NOSs for the concept that NO is a critical determinant of pulmonary vascular tone (6, 7, 9). Furthermore, pulmonary and total body NO are lower in IPAH patients as compared with healthy controls (3, 10–12), and the decrease of NO has been linked to increased arginase II and decreased eNOS expression in IPAH pulmonary endothelial cells *in vivo* (10, 13).

In addition to effects on vascular tone, NO regulates cellular bioenergetics through effects on glycolysis, oxygen consumption by mitochondrion, and mitochondrial biogenesis (14–17). For example, eNOS-deficient mice, which have mild pulmonary hypertension under normoxia and an exaggerated pulmonary vasoconstrictive response to hypoxia (18), have reduced mitochondria content in a wide range of tissues in association with significantly lower oxygen consumption and ATP content (14–17). Mitochondria are essential to cellular energy production in all higher organisms adapted to an oxygen-containing environment, i.e., ATP produced through oxidative phosphorylation. The electrochemical gradient used by mitochondrial F_0F_1 ATP synthase to synthesize ATP from ADP is generated by the proton pump action performed by Complexes I, III, and IV of the respiratory chain. The proton pumping is accompanied by electron shuttling, whereby Complexes I and II, along with the flavoprotein-ubiquinone oxidoreductase, transfer electrons from different sources to ubiquinone (coenzyme Q). The electrons are then transferred sequentially to Complex III, cytochrome *c*, Complex IV, and finally to molecular oxygen, the terminal electron acceptor. All multisubunit complexes of the respiratory chain (I–IV) are located in the mitochondrial inner membrane. Thus, mitochondria are the primary oxygen demand in the body, accounting for ≈90% of cellular oxygen consumption. Conversely, under limiting oxygen conditions, cells turn to glycolysis to generate energy. In endothelial cells, ATP is generated nearly equivalently by glycolysis and cellular respiration (19), accounting for a relative tolerance to hypoxia because of low oxygen demand and relatively high glycolytic activity (19, 20).

Interestingly, studies have identified site-specific defects in the electron transport chain in avian spontaneous idiopathic pulmonary hypertension; the lower respiratory chain coupling and inefficient use of oxygen have been linked to the development of pulmonary hypertension in avian species (21–23). Similarly, Fawn Hooded rats, a spontaneously pulmonary hypertensive rodent strain, have dysmorphic mitochondria with reduced expression of electron transport chain components. Dichloroacetate, a mitochondrial pyruvate dehydrogenase kinase inhibitor, prevents and reverses the pulmonary hypertension of Fawn Hooded rats, indicating a pathogenetic relation between mitochondria function and pulmonary hypertension (24, 25). Given

Author contributions: W.X., T.K., A.R.L., D.N., F.P.D., and S.C.E. designed research; W.X., T.K., A.R.L., F.P.D., M.K., A.J.J., F.A.M., A.C.A., C.J., R.A.D., and S.C.E. performed research; R.M.T. contributed new reagents/analytic tools; W.X., D.N., F.P.D., D.J.S., and S.C.E. analyzed data; and W.X. and S.C.E. wrote the paper.

The authors declare no conflict of interest.

This article is a PNAS direct submission.

Abbreviations: IPAH, idiopathic pulmonary arterial hypertension; PAH, pulmonary arterial hypertension related to risk factors or associated conditions; NOS, NO synthases; eNOS, endothelial NOS; MTT, 3-(4,5-dimethylthiazolyl-2)-2,5-diphenyltetrazolium bromide; PET, positron-emission tomography; CT, computed tomography; FDG, [^{18}F]fluoro-deoxy-D-glucose; SUV, standardized uptake values; LTF, lung tissue fraction; SNAP, *S*-nitroso-*N*-acetyl-D,L-penicillamine.

¶To whom correspondence should be addressed at: Cleveland Clinic, Lerner Research Institute, 9500 Euclid Avenue/NC22, Cleveland, OH 44195. E-mail: erzurus@ccf.org.

This article contains supporting information online at www.pnas.org/cgi/content/full/0605080104/DC1.

Table 1. Oxygen consumption of pulmonary artery endothelial cells

		Oxygen consumption*		Mitochondrial function
Substrate	Cell type	State 4	State 3	RCI
Glutamate-malate	Control PAEC	2.04 ± 0.10	5.44 ± 0.43	2.74 ± 0.20
Glutamate-malate	IPAH PAEC	1.28 ± 0.12†	3.36 ± 0.35†	2.65 ± 0.16
Succinate	Control PAEC	3.51 ± 0.25	9.40 ± 0.17	2.71 ± 0.23
Succinate	IPAH PAEC	1.83 ± 0.10†	4.76 ± 0.68†	2.60 ± 0.38

RCI, respiratory control index.

*Nanomoles of O_2 per minute per 10^6 cells; †, $P < 0.01$, $n = 4$ (IPAH), $n = 3$ (control), and $n = 8$ replicate experiments for substrates glutamate-malate, and $n = 5$ replicate experiments for substrate succinate.

these data and the low NO state of IPAH, we hypothesized that abnormalities of cellular metabolic energy pathways would be present in IPAH patients. To test this, oxygen consumption, ATP content, NO production, mitochondrial function, morphology and amount, and mitochondrial complexes activities were evaluated in pulmonary artery endothelial cells (PAEC) from IPAH and healthy control lungs. Subsequently, cellular glycolytic rate was determined in cells *in vitro*, and lung glycolytic rate was evaluated in patients with IPAH in comparison to healthy controls *in vivo*.

Results

Clinical Characteristics. Altogether, six controls, nine IPAH, and four PAH subjects were studied. PAEC were derived from donor lungs not used in transplantation and five IPAH and four PAH explanted lungs obtained at transplantation. Positron-emission tomography (PET)-computed tomography (CT) scans were conducted in three healthy female controls and four IPAH female patients. Clinical characteristics among subjects were similar [age (years): IPAH 45 ± 3, PAH 40 ± 4, control 35 ± 6; sex (female/male): IPAH 8/1, PAH 2/2, control 5/1; race (Caucasian/African American/Hispanic): IPAH 9/0/0, PAH 3/1/0, control 6/0/0]. Pulmonary hypertension was diagnosed by right heart catheterization performed for clinical care [pulmonary artery pressures (mmHg, 1 mmHg = 133 Pa): IPAH, systolic 94 ± 6, diastolic 41 ± 4, mean 59 ± 2; PAH, systolic 97 ± 12, diastolic 44 ± 14, mean 50 ± 6]. PAH was secondary to congenital heart diseases, except for one case of sarcoidosis. IPAH individuals were receiving vasodilators, anticoagulants, diuretics, digitalis, and/or oxygen by nasal cannula.

Decreased Oxygen Consumption in IPAH PAEC. To initially evaluate cellular respiration (21, 22), oxygen consumption in IPAH and control PAEC was determined. Compared with control cells ($n = 3$), IPAH PAEC ($n = 4$) had less oxygen consumption for state 3 and state 4 respirations with glutamate-malate or succinate as substrate (Table 1). However, the coupling between oxygen consumption and ATP production, the respiratory control index, was similar among IPAH and controls.

Activity and Expression of Mitochondrial Complexes. To determine causes of lower oxygen consumption, the activities of Complexes III and IV and the ability of mitochondria to reduce 3-(4,5-dimethylthiazolyl-2)-2,5-diphenyltetrazolium bromide (MTT) were determined (Fig. 1 *A* and *B*). Activity of Complex IV, the terminal enzyme complex of the respiratory chain that catalyzes the transfer of electrons from reduced cytochrome *c* to molecular oxygen, was significantly lower in IPAH PAEC ($n = 2$) than in control ($n = 2$), whereas Complex III activity was similar among the controls and IPAH cells (nanomoles of cytochrome *c* per minute per 10^6 cells: Complex IV, IPAH 9.83 ± 0.47, control 12.33 ± 0.73, $P < 0.05$, $n = 9$ replicate experiments, cells derived from each of two lungs from IPAH and controls in these series of experiments; Complex III, IPAH 5.65 ± 0.19, control 5.97 ± 0.22, $P > 0.05$, $n = 4$ replicate experiments) (Fig. 1*A*). MTT reduction by IPAH PAEC was strikingly lower than control, indicating less mitochondrial dehydrogenase activity (absorbance at 570 nm per 60,000 cells: IPAH 0.57 ± 0.03, control 0.75 ± 0.02, $P < 0.05$, $n = 9$ replicate experiments) (Fig. 1*B*).

Quantitation of mitochondria in electron microscopy images of cells (Fig. 1*C*) and Southern blot analysis of mtDNA (Fig. 1 *D* and *E*) revealed decreased mitochondrial numbers in IPAH PAEC compared with control (mitochondrial number per cell, IPAH 69 ± 7, control 191 ± 23, $P < 0.01$; mtDNA relative units per microgram of total DNA, IPAH 1 ± 0.16, control 2.29 ± 0.64, $P < 0.05$) but no discernible difference in mitochondrial morphology (Fig. 1*F*).

NO Production in IPAH PAEC. IPAH patients have low levels of exhaled NO (3, 11), and IPAH PAEC produce lower total amounts of NO products than control cells *in vitro* (10). Here, NO production by IPAH PAEC ($n = 3$) detected by measuring nitrite (NO_2^-) in the culture supernatants after ionomycin stimulation was also significantly lower than controls ($n = 3$, IPAH 0.30 ± 0.27, controls 3.91 ± 1.38 pmol/min per 10^6 cells, $P < 0.05$). Ionomycin-stimulated nitrite (NO_2^-) concentrations of IPAH and control cells were correlated to oxygen consumption for state 3 and state 4 respirations with glutamate-malate substrates (all $P < 0.01$) (Fig. 1*G*).

To test whether NO affects mitochondrial numbers and functions in IPAH cells, mitochondria numbers in electron microscopy images (Fig. 1*C*), mtDNA by Southern blot analysis (Fig. 1 *D* and *E*), and mitochondrial dehydrogenase activity were analyzed in IPAH cells ($n = 3$) after exposure to NO donors in culture. Mitochondrial numbers increased in IPAH PAEC after treatment with NO donors, DETA NONOate (detaNO), or *S*-nitroso-*N*-acetyl-D,L-penicillamine (SNAP) for 6 days compared with untreated cells (mitochondrial number/cell, untreated 69 ± 7, detaNO 93 ± 9, SNAP 90 ± 6, $P < 0.01$; mtDNA relative units per microgram of DNA, untreated 1 ± 0.16, detaNO 1.52 ± 0.47, SNAP 1.52 ± 0.40; $P = 0.06$ untreated vs. detaNO; $P < 0.05$ untreated vs. SNAP; $n = 3$) (Fig. 1 *C–F*). Mitochondrial dehydrogenase activity as measured by MTT also increased after NO donors (absorbance at 570 nm per 60,000 cells: untreated 0.42 ± 0.01, SNAP 0.49 ± 0.01, $P < 0.01$, $n = 3$), and Complex III-1 and cytochrome *c* protein levels were ≈2-fold greater after NO donors treatment (data not shown). Altogether, these data indicate that levels of NO in IPAH cells affect mitochondrial numbers and hence cellular bioenergetics in IPAH cells.

ATP Content in IPAH PAEC Under Normoxia (21% O_2) and Hypoxia (2% O_2). On the basis of the lower oxygen uptake and decreased mitochondrial function, we reasoned that the IPAH cells might have lower levels of energy production (20, 26, 27). To test this hypothesis, ATP content in IPAH ($n = 3$) and control cells ($n = 4$) was quantitated (Fig. 2*A*). Under 21% O_2, ATP content in IPAH cells was similar to controls ($P > 0.05$). Under hypoxia of 2% O_2,

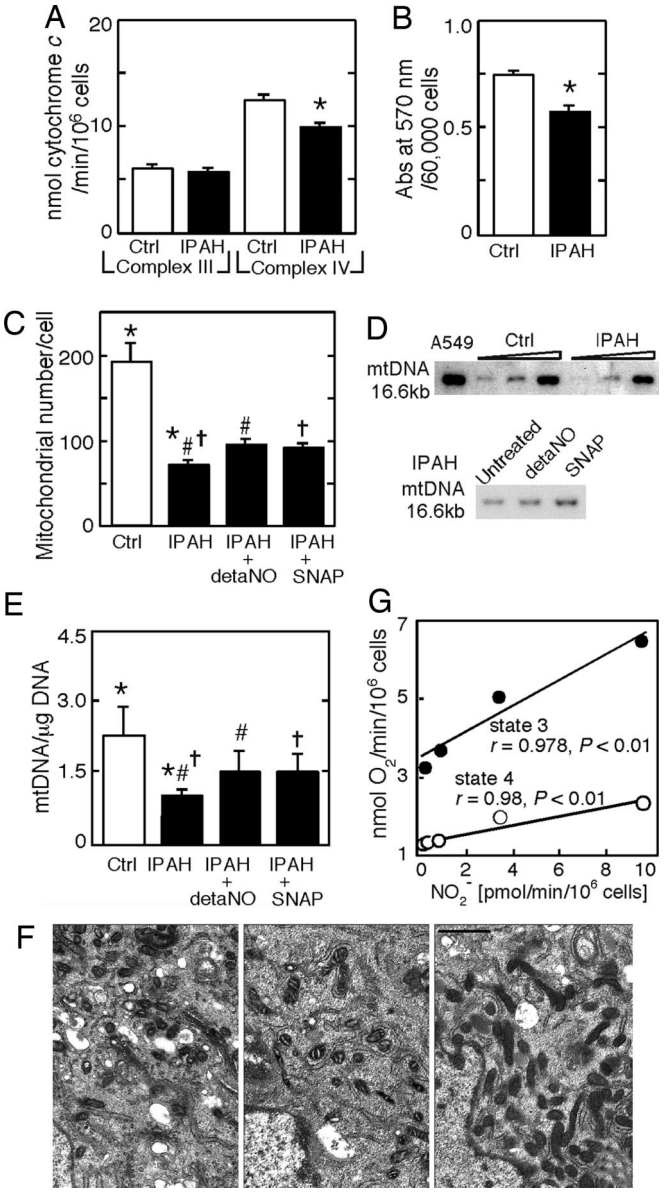

Fig. 1. Mitochondrial function, amount, and morphology. (*A*) Activities of mitochondrial Complexes III and IV of IPAH PAEC and healthy controls (*, $P < 0.05$, $n = 9$ replicate experiments). (*B*) Mitochondrial dehydrogenase activity of IPAH and control cells. MTT reduction (Abs at 570 nm per 60,000 cells) by IPAH cells was lower than control (*, $P < 0.05$, $n = 9$ replicate experiments). (*C*) Mitochondrial number per cell by electron microscopy in untreated IPAH and healthy control PAEC and IPAH PAEC exposed to NO donors, DETA NONOate (detaNO), or SNAP (*, #, †, $P < 0.01$). (*D*) Southern blot analysis of mtDNA content in IPAH PAEC. (*Upper*) Each lane contains increasing total DNA from PAEC loaded at 1, 3, or 10 μg or from A549 cells (10 μg). (*Lower*) Total DNA (5 μg per lane) from IPAH PAEC with NO donors. (*E*) mtDNA relative units per microgram of DNA in untreated IPAH and healthy control and in IPAH exposed to NO donors (*, †, $P < 0.05$; #, $P = 0.06$). (*F*) Ultrastructure detail of mitochondria in untreated IPAH PAEC (*Center*), healthy control (*Left*), and IPAH exposed to detaNO (*Right*). (Scale bar: 1 μm.) (*G*) Endogenous NO production and cell respiration. Correlation of nitrite (NO_2^-) concentrations in the culture supernatants from ionomycin-treated cells (picomoles per minute per 10^6 cells) and oxygen consumption (nanomoles of O_2 per minute per 10^6 cells) for state 3 ($n = 4$) and state 4 ($n = 5$) respirations from concurrent cultured IPAH and healthy control cells. Symbols in figures identify the comparison pairs for multiple comparisons, and the *P* values are noted in the text.

ATP content in control cells dropped by >30% ($P < 0.01$), but ATP content in IPAH PAEC exhibited similar levels under normoxia ($P > 0.05$) (relative ATP content: normoxia, IPAH 0. 91 ± 0.03, control 1.00 ± 0.02; hypoxia, IPAH 0.81 ± 0.04, control 0.64 ± 0.03; $n = 14$ replicate experiments) (Fig. 2*A*).

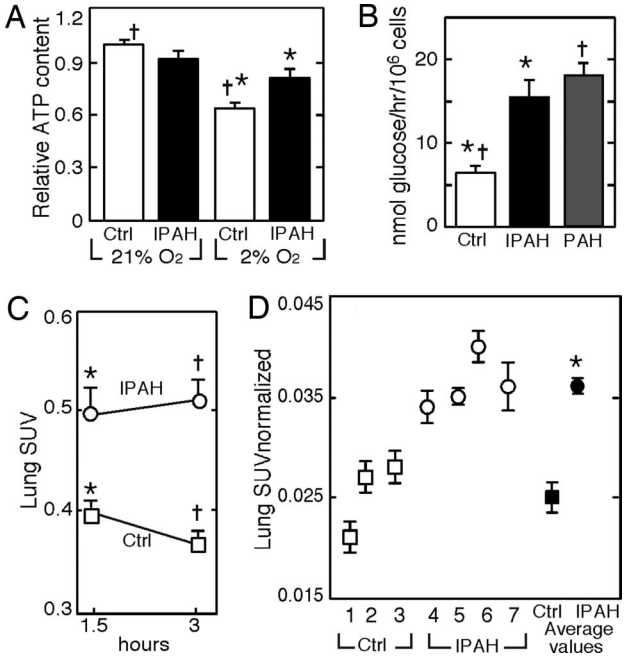

Fig. 2. ATP content and glycolytic rate *in vitro* and glucose metabolic activities *in vivo*. (*A*) Under normoxia (21% O_2), ATP content in IPAH PAEC ($n = 4$) was similar to controls ($n = 3$). Under hypoxia (2% O_2), ATP content in IPAH PAEC ($n = 4$) was significantly higher than controls ($n = 3$) but similar to the value under normoxia (*,†, $P < 0.01$, $n = 14$ replicate experiments; ATP values shown are relative to values of control cells under normoxia). (*B*) Glycolytic rate from IPAH PAEC ($n = 5$) or from PAH PAEC ($n = 4$) was higher than healthy controls ($n = 3$, *, †, $P < 0.01$). (*C*) SUV of FDG-PET scan in lungs of IPAH patients ($n = 4$) and healthy controls ($n = 3$) at 1.5 and 3 h after injection (*, †, $P < 0.01$). (*D*) Glucose metabolic activities in lungs of IPAH patients were higher than in healthy controls (*, $P < 0.01$) in four IPAH patients (subjects 4–7) as compared with three healthy controls (subjects 1–3). The 3-h SUV was normalized to LTF. Symbols in figures identify the comparison pairs for multiple comparisons, and the *P* values are noted in the text.

Increased Glycolytic Rate in IPAH PAEC. The greater tolerance to hypoxia indicates that IPAH PAEC have a lesser dependence on cellular respiration for energy than control cells and suggests a predominant anaerobic cellular energy source. Thus, the ^{3}H-glucose glycolytic rate in IPAH was compared with control cells. The glycolytic rate of IPAH PAEC ($n = 5$) was significantly higher than controls ($n = 3$) (nanomoles per hour per 10^6 cells, IPAH 15.4 ± 1.9, controls 6.2 ± 0.84, $P < 0.01$), and lactate release was ≈1.5-fold higher from IPAH PAEC ($n = 3$) compared with controls ($n = 3$), indicating that glucose metabolism was subserving the primary role for energy requirements. Interestingly, glycolytic rate of PAH PAEC ($n = 4$) was also significantly higher than controls ($n = 3$) (nanomoles per hour per 10^6 cells, PAH 18.2 ± 1.3, controls 6.2 ± 0.84, $P < 0.01$) (Fig. 2*B*).

Glucose Metabolic Activities Determined by PET Scan of Lungs. IPAH is pathologically characterized by proliferative vascular endothelial lesions in the size of ≈150 μm (1, 2). Because cellular energy metabolism in IPAH appeared reliant on glycolysis, a situation similar to alterations noted in cancer cell bioenergetics and used in cancer screening technologies, we reasoned that we might see a difference in the glucose analogue tracer [^{18}F]fluoro-deoxy-D-glucose (FDG) uptake into pulmonary vascular endothelial cells, i.e., FDG-PET scan. The glucose analogue tracer [^{18}F]FDG is taken

up into cells by glucose transporters, phosphorylated to [^{18}F]FDG-6-P in the presence of hexokinase, but unlike glucose, is trapped within cells with no further metabolism because of the lack of the hydroxyl group in the second carbon position (28). Here, although FDG-PET spatial resolution limits are at 6 mm^3, given the extensive nature of the pulmonary vascular disease in IPAH, FDG-PET scan was used to evaluate whether glucose metabolism was increased diffusely in the lungs of four IPAH patients and three healthy controls (Fig. 2 *C* and *D* and supporting information (SI) Fig. 3). Lung standardized uptake values (SUV) of IPAH patients were significantly higher than healthy controls at [^{18}F]FDG uptake times of 1.5 and 3 h. IPAH lung SUV increased at 3 h compared with SUV at 1.5 h (1.5-h lung SUV, IPAH 0.496 ± 0.030, control 0.397 ± 0.013, $P < 0.01$; 3-h lung SUV, IPAH 0.511 ± 0.023, control 0.367 ± 0.015, $P < 0.01$) (Fig. 2*C*), whereas there was no significant difference in liver SUV among IPAH and controls at either 1.5 or 3 h (1.5-h liver SUV, IPAH 2.023 ± 0.133, control 1.895 ± 0.058; 3-h liver SUV, IPAH 1.853 ± 0.072, control 1.693 ± 0.075; all $P > 0.05$). To distinguish between increase in glycolysis and increased endothelial cell mass, lung tissue fraction (LTF), which represents lung tissue density, was measured from lungs of IPAH patients and healthy controls. In contrast to SUV, LTF of IPAH patients was similar to healthy controls (1.5-h LTF, IPAH 0.256 ± 0.015, control 0.238 ± 0.008, $P = 0.298$; 3-h lung LTF, IPAH 0.265 ± 0.012, control 0.244 ± 0.007, $P = 0.156$). Thus, glucose metabolic activities relative to lung density, i.e., SUV normalized with LTF, were greater in IPAH than in healthy controls (SUV normalized at 3 h, IPAH 0.036 ± 0.001, control 0.025 ± 0.002, $P < 0.01$) (Fig. 2*D*).

Given the similar LTF of IPAH and control lungs but significantly higher glucose uptake in IPAH lungs and the increase of SUV only in IPAH lungs over time, the *in vivo* findings most likely reflect an increased glycolytic rate rather than increased endothelial cell mass, which would be consistent with the *in vitro* glycolytic rate studies.

Discussion

Mitochondrial defects have been found in a wide variety of human diseases, e.g., Huntington disease, Parkinson disease, Friedreich's ataxia, as well as in cancer (29). Here, we show abnormalities of energy metabolism in IPAH pulmonary endothelial cells, including lower oxygen consumption of mitochondria and significantly higher glycolytic rate. Tumor cells often exhibit this same combination of alterations in cellular energy production, a phenomenon first described more than 80 years ago and known as the Warburg effect (30). Characteristically, poorly differentiated cancers, cancers with higher incidence of metastases, and/or rapidly growing tumors have higher glycolytic rates even under plentiful O_2 conditions (31, 32). The condition of aerobic glycolysis is not a unique feature of tumor cells but is also found in nontransformed rapidly proliferating cells when sufficient glucose is available (33). Thus, aerobic glycolysis has been linked primarily to rapid cell proliferation rather than to malignancy (33). The occurrence of aerobic glycolysis, or the Warburg effect, in IPAH endothelial cells is consistent with the increased proliferative capacity of these cells in the pulmonary vascular lesions of IPAH (34).

Aerobic glycolysis, which yields two ATP per glucose as opposed to complete oxidation that produces 38 ATP per glucose, can meet the enhanced ATP demand of proliferating cells but far less effectively (33). However, aerobic glycolysis is likely advantageous to rapidly growing cells because it renders them less dependent on oxygen, thereby improving their survival in an environment that may become hypoxic as cell numbers increase. Further, the transition to aerobic glycolysis by proliferating cells minimizes exposure to reactive oxygen species, i.e., diminished oxidative metabolism (35, 36). Despite many years of investigation, however, it is still unclear as to what regulatory mechanisms transition proliferating cells from oxidative glucose metabolism to anaerobic glycolysis (33). Recent studies indicate that glycolytic conversion of bioenergetics in cells is an early pretransformation event and can be triggered by p53, a gene commonly mutated in cancers (37–39). It has also been speculated that decreased mitochondrial function may be a primary stimulus to glycolysis (20, 40). In this context, NO binds to several targets within the mitochondrial respiratory chain, e.g., Complex I, Complex II, and Complex IV, and inhibits their functions (41, 42). On this basis, mitochondrial function and cellular respiration would be expected to increase in the condition of low NO in IPAH. However, NO also has other long-term effects on mitochondrial biogenesis and function in cells (14–17), e.g., NO/cGMP-dependent mitochondrial biogenesis is associated with enhanced coupled respiration, oxygen consumption, and ATP content (14–17). Here, decreased mitochondria functional activities in the context of preserved respiratory control index in IPAH cells suggested that decreased activity was not due to mitochondrial dysfunction. In fact, mitochondrial numbers in IPAH cells were low. On the other hand, studies of spontaneous pulmonary hypertension in avian and rodent species identify intrinsic deficiencies in mitochondrial function rather than numbers (21, 25). Taken together, these data indicate that decreased mitochondrial function, whether related to lower numbers of mitochondria and/or an intrinsic impairment of function, is associated with pulmonary hypertension. The relation of endogenous NO to cellular respiration and the increase of mitochondrial numbers after NO donor confirm that NO plays a role in regulating mitochondrial biogenesis and bioenergetics (20, 40). However, the similar glycolytic activity of IPAH and PAH, although NO production is not altered in PAH (11), suggests other mechanisms also modify cell bioenergetics, such as inflammation or pressure and/or flow effects. Inflammatory necrotizing arteritis, infiltration of macrophages and lymphocytes into pulmonary vasculature (43), and high serum levels of proinflammatory cytokines are typically present in PAH patients (44). In this context, TNFα impairs both mitochondrial biogenesis and function by down-regulating eNOS expression (45). Thus, changes in the mitochondrial function and number may coexist in PAH pathophysiology.

Nevertheless, our findings identify a switch to energy derived from primarily glycolytic metabolism in human pulmonary hypertension, a situation similar to the abnormalities identified in avian and rodent pulmonary hypertension and analogous to alterations in cancer cell metabolism. The potential clinical utility of this finding includes possibilities such as using glucose uptake to monitor treatment response, to provide complementary but unique information to measures of pulmonary artery pressure and/or cardiac function. The detectable greater glucose uptake by FDG-PET suggests that as volumetric resolution technology improves, PET scanning may be used in quantitative analyses of IPAH vascular lesions. Although serial determination of pulmonary artery pressures is performed in the clinical care of patients, currently there is no method to evaluate endothelial cell proliferative responses to therapy over time. Increase of glucose uptake by IPAH cells may also serve as a biologic target for novel drug delivery. Overall, the findings in this study support that there is a fundamental alteration in cellular bioenergetics in IPAH, linking the human disease to avian and rodent forms of PAH, species in which inefficient cellular use of oxygen has been shown to predispose them to development of pulmonary hypertension (32).

Materials and Methods

Study Population. IPAH patients were identified by the revised clinical classification of pulmonary hypertension (Venice 2003) (46). The study was approved by the Cleveland Clinic Institu-

tional Review Board, and written informed consent was obtained from individuals.

Cell Culture. Human PAEC were dissociated and cultured as described in *SI Text*. A549 cells, an epithelial cell line derived from lung adenocarcinoma, were cultured in MEM (Invitrogen Corporation, Carlsbad, CA) with 10% heat-inactivated FCS. Cells were subjected to hypoxia in a sealed chamber with 2% O_2, 5% CO_2, and 93% N_2 or placed directly in a 5% CO_2 and 95% air incubator (20% O_2) and cultured at 37°C. For NO donor treatment, 125 μM detaNO or 100 μM SNAP was added once a day to cell culture from day 1 to day 6 (15).

Detection of Endothelium-Derived NO. To evaluate NO synthesis, nitrite (NO_2^-) concentrations in the culture supernatants were measured in ionomycin-stimulated cell supernatant from subconfluent PAEC from IPAH lung or control lung as described (10). Nitrite concentrations were determined by using the ISO-NOP Nitric Oxide Sensor (World Precision Instruments, Sarasota, FL), an amperometric sensor specific for NO.

Mitochondrial Respiration. Oxygen consumption of cells vs. healthy controls was measured at 37°C in circulator chambers by using an 5300A biological oxygen monitor (YSI, Yellow Springs, OH) and Clark-type polarographic oxygen electrodes as described with slight modifications (47). Briefly, reactions were conducted using 0.01% digitonin (wt/vol) (Sigma-Aldrich, St. Louis, MO) permeabilized PAEC (7.5×10^6 cells in 3-ml reaction volume) in a reaction medium [250 mM sucrose, 20 mM D-glucose, 40 mM KCl, 5 mM KH_2PO_4, 3 mM $MgCl_2$, 0.5 mM EDTA, 30 mM Tris·HCl, pH 7.5, and protease inhibitors aprotinin (5 μg/ml), leupeptin (1 μg/ml), pepstatin (1 μg/ml), and Pefabloc SC (24 μg/ml)]. Oxygen consumption measurements were made under state 3 and state 4 respiration using either 5 mM glutamate and 2.5 mM malate or 5 mM succinate as substrate. State 3 respiration was stimulated by the addition of 1 mM ADP. The respiratory control index was calculated by dividing oxygen consumption rate at state 3 by state 4.

Respiratory Chain Complex Assays. The activities of Complex III and IV of the mitochondrial respiratory chain were measured spectrophotometrically as described (48). Briefly, cells (20×10^6 per ml) were incubated with 0.01% digitonin (Sigma-Aldrich) in PBS containing protease inhibitors [5 μg/ml aprotinin, 1 μg/ml leupeptin, 1 μg/ml pepstatin, and 24 μg/ml Pefabloc SC (Sigma-Aldrich)] (pH 7.4) for 5 min on ice. After centrifugation at $16,000 \times g$ and 4°C for 1 min, the supernatant, containing cytosolic proteins, was removed, and the organelle pellet was resuspended in an equal amount of assay buffer. For Complex III and Complex IV activity, an organelle volume correlating to 40,000 and 10,000 cells was used per reaction, respectively. Complex III activity was measured at 550 nm and 30°C with 15 μM cytochrome *c* (III), 0.6 mM *n*-dodecyl-β-D-maltoside (EMD Biosciences, Inc., La Jolla, CA), 2 μg/ml rotenone, and 35 μM ubiquinol in assay medium [25 mM potassium phosphate, 5 mM $MgCl_2$, 2 mM KCl, 2.5 mg/ml BSA (fraction V), pH 7.2]. Ubiquinol was prepared by dissolving ubiquinone (10 μmol) in 1 ml of ethanol acidified to pH 2 with 6 M HCl. The quinone was reduced with excess solid sodium borohydride. Ubiquinol was extracted into diethylether/cyclohexane (2:1, vol/vol), evaporated to dryness under nitrogen gas, and redissolved in 1 ml of ethanol acidified to pH 2 with 6 M HCl. For Complex IV activity, cytochrome *c* was reduced with 1 M ascorbate in 0.1 M Mes (pH 7.0) for 20 min and desalted afterward by using a D-Salt Excellulose GF-5 column (Pierce Biotechnology, Inc., Rockford, IL). Complex IV activity was measured at 550 nm and 25°C with 15 μM cytochrome *c* (II), 0.45 mM *n*-dodecyl-β-D-maltoside in 20 mM potassium phosphate (pH 7.0).

MTT Assay. Mitochondrial dehydrogenase activity in cells was determined by the ability of mitochondria to reduce MTT according to the protocol from American Type Culture Collection (Manassas, VA). Absorbance at 570 nm was measured.

ATP Content in IPAH PAEC. ATP in cells was measured under normoxia (21% O_2) or hypoxia (2% O_2) for 4 h by using a luciferase-based luminescence assay kit (PerkinElmer, Boston, MA).

Glycolytic Rate. Glycolytic rate of cells was measured by monitoring the conversion of 5-^{3}H-glucose to ^3H_2O (49, 50). Briefly, 2×10^5 PAEC from IPAH or healthy controls were suspended in 0.2 ml of endothelial cell growth medium (EGM-2 containing 1,000 mg/L glucose; Cambrex, Walkersville, MD), and 10 μl of 5-^{3}H-glucose (PerkinElmer Life Sciences Inc., Boston, MA) was added to each well. Samples were incubated for 1 h at 37°C in a humidified incubator under 5% CO_2. Reactions were terminated with 0.5 ml of 0.2 N HCl, and 100 μl of the cell/HCl mixture was added to open tubes, which were then placed upright in 4-ml scintillation vials containing 0.5 ml of H_2O. The vials were capped, sealed with parafilm, and incubated for 2 days at room temperature. During the incubation, ^3H_2O generated by glycolysis diffused from the tube to the H_2O in the scintillation vial through evaporation and condensation. The contents of the tube were transferred to a new scintillation vial with 0.5 ml of H_2O, the tube was discarded, and scintillation fluid was added to both the original (diffused counts) and second (undiffused counts) vials. The amounts of diffused and undiffused ^{3}H were determined by scintillation counting. Appropriate ^{3}H-glucose-only and ^3H_2O-only controls were included, enabling the calculation of ^3H_2O in each sample and thus the rate of glycolysis as described (49). Lactate concentration in supernatants overlying culture cells was determined spectrophotometrically (Trinity Biotech, St. Louis, MO). Lactate was converted to pyruvate and hydrogen peroxide (H_2O_2) by lactate oxidase. H_2O_2 in the presence of a peroxidase subsequently catalyzes oxidative condensation of a precursor, producing a chromogen with an absorption maximum at 540 nm.

Southern Blot Analysis. Total DNA was extracted from cultured cells (Qiagen Inc., Valencia, CA). Primers (5′-TGATCAGAG-GATTGAGTAAACGG-3′ and 5′-GGTACCCTAACCGTGCAA-AGGTA-3′) were used to amplify a 1,090-bp DNA fragment (2,574–3,663 bp; GenBank accession no. AY339547) from 16,569-bp human mitochondrial genomic DNA (51). The PCR products were purified, sequenced, and used as a probe for Southern blot analysis. For Southern blot analysis, the amount of total DNA from cultured cells was digested with restriction enzyme PvuII, electrophoresed through a 0.8% agarose gel, and transferred to Duralon-UV membranes (Stratagene, Cedar Creek, TX). The filters were hybridized with the ^{32}P-labeled PCR-generated mitochondrial DNA (mtDNA) probe and visualized with autoradiography.

Ultrastructural Analyses. Cells were fixed at 4°C for >1 h in 0.1 M sodium cacodylate buffer (pH 7.4) containing 2.5% glutaraldehyde and 4% formaldehyde. After washing three times in the same buffer, cells were postfixed with 1% aqueous osmium tetroxide for 1 h at 4°C, washed in sodium cacodylate buffer, followed by maleate buffer (pH 5.1), and then dehydrated with ascending grades of ethanol and propylene oxide. Samples were embedded in Eponate12 kit, polymerized at 70°C for 48 h, trimmed, sectioned at 70–90 nm, poststained in saturated uranyl acetate and lead citrate, and examined with a transmission electron microscope (Philips CM12; Philips, Eindhoven, The Netherlands).

PET Scan. The study subjects were imaged sequentially by using x-ray CT and PET on a combined hybrid PET/CT system (Biograph 16 PET/CT; Siemens Medical Solutions, Knoxville, TN) (52). The system is calibrated so that the CT and PET data are coregistered, resulting in fused anatomic and functional images.

Subjects were fasting for at least 6 h before and during the study. For each subject, a 370-MBq (10-mCi) dose of FDG was administered through i.v. injection. With the subject in a resting state, time was allowed for uptake of FDG before commencing imaging. For four of the seven subjects, imaging was performed at 1.5 and 3 h after injection. For the other three of the seven subjects, imaging was performed at 3 h after injection. Differing uptake times were used with the goal of optimizing the lung tissue uptake relative to background activity to enhance the differences between study and control subjects. The underlying hypothesis was that a longer uptake time would allow for more clearance of activity from the blood, whereas phosphorylated FDG would remain trapped in tissue cells.

Image data were analyzed by a nuclear medicine radiologist (D.N.) by using an image fusion workstation (MSViewer; CPS Innovations, Knoxville, TN) with region-of-interest (ROI) measuring tools. Identical ROIs were placed on the several regions on fused CT and PET images, and the mean CT Hounsfield units (HU) and mean PET SUV were recorded. A total of 10 regions were drawn in the lungs, at upper/mid/lower levels and anterior/posterior of each lung. Regions were also drawn in the liver (upper/mid/lower levels) and within the aorta (ascending/arch/descending). LTF, which represents lung tissue density, was calculated by using the following formula: LTF = (1,000 + HU of lung)/1,000. To account for variations in lung tissue density and FDG distribution (e.g., muscular uptake) between patients, SUV of each region of the lung was then normalized for LTF of lung and HU of liver by using the following formula: SUV normalized = SUV of each region of the lung/LTF lung of same region/mean HU of liver.

We thank Mei Yin for ultrastructural analyses, Tannishia M. Goggans for cell culture, Daniel Laskowski for hypoxic condition, and Kirk B. Lane for kindly providing tissue.

1. Jeffery TK, Morrell NW (2002) *Prog Cardiovasc Dis* 45:173–202.
2. Archer S, Rich S (2000) *Circulation* 102:2781–2791.
3. Kaneko FT, Arroliga AC, Dweik RA, Comhair SA, Laskowski D, Oppedisano R, Thomassen MJ, Erzurum SC (1998) *Am J Respir Crit Care Med* 158:917–923.
4. Azeka E, Costa Auler JO, Jr, Kajita L, Alliman AC, Franchini Ramires JA, Ebaid M (2002) *Pediatr Cardiol* 23:20–26.
5. Cooke JP, Dzau VJ (1997) *Circulation* 96:379–382.
6. Ignarro LJ (1993) *Thromb Haemost* 70:148–151.
7. Moncada S (1999) *J R Soc Med* 92:164–169.
8. Forstermann U, Schmidt HH, Pollock JS, Sheng H, Mitchell JA, Warner TD, Nakane M, Murad F (1991) *Biochem Pharmacol* 42:1849–1857.
9. Champion HC, Bivalacqua TJ, Greenberg SS, Giles TD, Hyman AL, Kadowitz PJ (2002) *Proc Natl Acad Sci USA* 99:13248–13253.
10. Xu W, Kaneko FT, Zheng S, Comhair SA, Janocha AJ, Goggans T, Thunnissen FB, Farver C, Hazen SL, Jennings C, *et al.* (2004) *FASEB J* 18:1746–1748.
11. Ozkan M, Dweik RA, Laskowski D, Arroliga AC, Erzurum SC (2001) *Lung* 179:233–243.
12. Girgis RE, Champion HC, Diette GB, Johns RA, Permutt S, Sylvester JT (2005) *Am J Respir Crit Care Med* 172:352–357.
13. Giaid A, Saleh D (1995) *N Engl J Med* 333:214–221.
14. Nisoli E, Falcone S, Tonello C, Cozzi V, Palomba L, Fiorani M, Pisconti A, Brunelli S, Cardile A, Francolini M, *et al.* (2004) *Proc Natl Acad Sci USA* 101:16507–16512.
15. Nisoli E, Clementi E, Paolucci C, Cozzi V, Tonello C, Sciorati C, Bracale R, Valerio A, Francolini M, Moncada S, Carruba MO (2003) *Science* 299:896–899.
16. Momken I, Fortin D, Serrurier B, Bigard X, Ventura-Clapier R, Veksler V (2002) *Biochem J* 368:341–347.
17. Clementi E, Nisoli E (2005) *Comp Biochem Physiol A Mol Integr Physiol* 142:102–110.
18. Fagan KA, Fouty BW, Tyler RC, Morris KG, Jr, Hepler LK, Sato K, LeCras TD, Abman SH, Weinberger HD, Huang PL, *et al.* (1999) *J Clin Invest* 103:291–299.
19. Culic O, Gruwel ML, Schrader J (1997) *Am J Physiol* 273:C205–C213.
20. Loike JD, Cao L, Brett J, Ogawa S, Silverstein SC, Stern D (1992) *Am J Physiol* 263:C326–C333.
21. Tang Z, Iqbal M, Cawthon D, Bottje WG (2002) *Comp Biochem Physiol A Mol Integr Physiol* 132:527–540.
22. Iqbal M, Cawthon D, Wideman RF, Jr, Bottje WG (2001) *Poult Sci* 80:485–495.
23. Cawthon D, Iqbal M, Brand J, McNew R, Bottje WG (2004) *Poult Sci* 83:259–265.
24. Michelakis ED, McMurtry MS, Wu XC, Dyck JR, Moudgil R, Hopkins TA, Lopaschuk GD, Puttagunta L, Waite R, Archer SL (2002) *Circulation* 105:244–250.
25. Bonnet S, Michelakis ED, Porter CJ, Andrade-Navarro MA, Thebaud B, Haromy A, Harry G, Moudgil R, McMurtry MS, Weir EK, Archer SL (2006) *Circulation* 113:2630–2641.
26. Janssens D, Michiels C, Delaive E, Eliaers F, Drieu K, Remacle J (1995) *Biochem Pharmacol* 50:991–999.
27. Piper HM, Noll T, Siegmund B (1994) *Cardiovasc Res* 28:1–15.
28. Chen DL, Richard JC, Schuster DP (2004) *Methods Enzymol* 385:315–333.
29. Schapira AH (1999) *Biochim Biophys Acta* 1410:159–170.
30. Warburg O, Posener K, Negelein E (1924) *Biochem Z* 152:319–344.
31. Weinhouse S (1972) *Cancer Res* 32:2007–2016.
32. Gatenby RA, Gillies RJ (2004) *Nat Rev Cancer* 4:891–899.
33. Wang T, Marquardt C, Foker J (1976) *Nature* 261:702–705.
34. Cool CD, Groshong SD, Oakey J, Voelkel NF (2005) *Chest* 128:565S–571S.
35. Andrae U, Singh J, Ziegler-Skylakakis K (1985) *Toxicol Lett* 28:93–98.
36. O'Donnell-Tormey J, Nathan CF, Lanks K, DeBoer CJ, de la Harpe J (1987) *J Exp Med* 165:500–514.
37. Garber K (2006) *Science* 312:1158–1159.
38. Matoba S, Kang J, Patino W, Wragg A, Boehm M, Gavrilova O, Hurley P, Bunz F, Hwang P (2006) *Science* 16:1650–1653.
39. Ramanathan A, Wang C, Schreiber SL (2005) *Proc Natl Acad Sci USA* 102:5992–5997.
40. Merlo-Pich M, Deleonardi G, Biondi A, Lenaz G (2004) *Exp Gerontol* 39:277–281.
41. Antunes F, Boveris A, Cadenas E (2004) *Proc Natl Acad Sci USA* 101:16774–16779.
42. Ramachandran A, Levonen AL, Brookes PS, Ceaser E, Shiva S, Barone MC, Darley-Usmar V (2002) *Free Radic Biol Med* 33:1465–1474.
43. Tuder RM, Groves B, Badesch DB, Voelkel NF (1994) *Am J Pathol* 144:275–285.
44. Humbert M, Monti G, Brenot F, Sitbon O, Portier A, Grangeot-Keros L, Duroux P, Galanaud P, Simonneau G, Emilie D (1995) *Am J Respir Crit Care Med* 151:1628–1631.
45. Valerio A, Cardile A, Cozzi V, Bracale R, Tedesco L, Pisconti A, Palomba L, Cantoni O, Clementi E, Moncada S, *et al.* (2006) *J Clin Invest* 116:2791–2798.
46. Simonneau G, Galie N, Rubin LJ, Langleben D, Seeger W, Domenighetti G, Gibbs S, Lebrec D, Speich R, Beghetti M, *et al.* (2004) *J Am Coll Cardiol* 43:5S–12S.
47. Koeck T, Fu X, Hazen SL, Crabb JW, Stuehr DJ, Aulak KS (2004) *J Biol Chem* 279:27257–27262.
48. Birch-Machin MA, Turnbull DM (2001) *Methods Cell Biol* 65:97–117.
49. Ashcroft SJ, Weerasinghe LC, Bassett JM, Randle PJ (1972) *Biochem J* 126:525–532.
50. Edinger AL, Thompson CB (2004) *Oncogene* 23:5654–5663.
51. Anderson S, Bankier AT, Barrell BG, de Bruijn MH, Coulson AR, Drouin J, Eperon IC, Nierlich DP, Roe BA, Sanger F, *et al.* (1981) *Nature* 290:457–465.
52. Wong WL, Campbell H, Saunders M (2002) *Clin Oncol (R Coll Radiol)* 14:123–128.